



Search for Hydrogenated C₆₀ (Fulleranes) in Circumstellar Envelopes

Yong Zhang (张泳)^{1,2}, SeyedAbdolreza Sadjadi¹, Chih-Hao Hsia (夏志浩)^{1,2,3}, and Sun Kwok (郭新)^{1,4,5}

¹ Laboratory for Space Research, Faculty of Science, The University of Hong Kong, Pokfulam Road, Hong Kong, China; sunkwok@hku.hk

² Department of Physics, The University of Hong Kong, Pokfulam Road, Hong Kong, China

³ Space Science Institute, Macau University of Science and Technology, Avenida Wai Long, Taipa, Macau, China

⁴ Department of Earth Sciences, The University of Hong Kong, Pokfulam Road, Hong Kong, China

⁵ Visiting Professor, Department of Physics and Astronomy, University of British Columbia, Vancouver, B.C., Canada

Received 2016 November 23; revised 2017 May 1; accepted 2017 May 2; published 2017 August 14

Abstract

The recent detection of fullerene (C₆₀) in space and the positive assignment of five diffuse interstellar bands to C₆₀⁺ reinforce the notion that fullerene-related compounds can be efficiently formed in circumstellar envelopes and be present in significant quantities in the interstellar medium. Experimental studies have shown that C₆₀ can be readily hydrogenated, raising the possibility that hydrogenated fullerenes (or fulleranes, C₆₀H_m, m = 1–60) may be abundant in space. In this paper, we present theoretical studies of the vibrational modes of isomers of C₆₀H_m. Our results show that the four mid-infrared bands from the C₆₀ skeletal vibrations remain prominent in slightly hydrogenated C₆₀, but their strengths diminish in different degrees with increasing hydrogenation. It is therefore possible that the observed infrared bands assigned to C₆₀ could be due to a mixture of fullerenes and fulleranes. This provides a potential explanation for the observed scatter of the C₆₀ band ratios. Our calculations suggest that a feature around 15 μm due to the breathing mode of heavily hydrogenated C₆₀ may be detectable astronomically. A preliminary search for this feature in 35 C₆₀ sources is reported.

Key words: astrochemistry – circumstellar matter – infrared: stars – ISM: lines and bands

Supporting material: animation, data behind figures

1. Introduction

It is now well established that circumstellar envelopes are major sources of molecules and solids in the Galaxy. Recent infrared and millimeter-wave observations have shown that complex molecules can be efficiently synthesized in circumstellar envelopes of evolved stars, ejected into the interstellar medium, and distributed throughout the Galaxy (Kwok 2004). The discovery of pre-solar grains carrying isotopic signatures of asymptotic giant branch stars offers proof that products of circumstellar chemical synthesis did survive the journey across the Galaxy and can be embedded in the early solar system (Zinner 1998). Among the molecules synthesized in the circumstellar environment is the pure carbon molecule fullerene (C₆₀). Circumstellar C₆₀ was first discovered through its four vibrational bands in the young planetary nebula Tc1 (Cami et al. 2010). Subsequently, the C₆₀ vibrational bands have been detected in a variety of circumstellar environments (García-Hernández et al. 2010, 2011, 2011b; Sellgren et al. 2010; Gielen et al. 2011; Zhang & Kwok 2011; Evans et al. 2012; Roberts et al. 2012; Otsuka et al. 2013), although the excitation and formation mechanisms of circumstellar C₆₀ remain unclear (e.g., Zhang & Kwok 2013, and references therein). Specifically, C₆₀ has been detected in 11, 4, and 7 planetary nebulae in the Galaxy, the Large Magellanic Cloud (LMC), and Small Magellanic Cloud (SMC), respectively, and the detection rate is highest among the SMC planetary nebulae, followed by LMC and Galactic planetary nebulae (García-Hernández et al. 2012; Otsuka et al. 2016). Some of the C₆₀ sources also exhibit vibrational bands from C₆₀⁺ (Berné et al. 2013; Zhang & Kwok 2013; Strelnikov et al. 2015).

Since its first synthesis in the laboratory, C₆₀ or its derivatives have been speculated to be abundant in the interstellar medium and may serve as the carrier of the diffuse interstellar bands (DIBs; Kroto et al. 1985). However, the

search for electronic transitions of C₆₀ in space has not been successful (Snow & Seab 1989; Herbig 2000), suggesting that interstellar C₆₀ (if any) might have been converted into other molecular forms. Based on the laboratory spectra recorded in a neon matrix (Fulara et al. 1993), Foing & Ehrenfreund (1994) ascribed two strong DIBs at 9632 and 9577 Å to C₆₀⁺. This identification has remained uncertain due to a lack of gas-phase experimental data and the non-detection of other DIBs coinciding with weaker C₆₀⁺ bands. Recently, Campbell et al. (2015) reported the cold gas-phase spectrum of C₆₀⁺, which exhibits features remarkably consistent with the two DIBs not only for the wavelengths but also for the bandwidths and relative intensities (see also Campbell et al. 2016a). The weaker C₆₀⁺ bands at 9348.4, 9365.2, and 9427.8 Å were soon thereafter discovered in diffuse clouds (Walker et al. 2015; Campbell et al. 2016b). Thus far five DIBs have been convincingly assigned to C₆₀⁺.

The same C₆₀⁺ absorption bands at 9632 and 9577 Å have been detected with remarkably large equivalent widths toward a C₆₀-containing proto-planetary nebula IRAS 01005+7910 by Iglesias-Groth & Esposito (2013), suggesting that these two bands are primarily of circumstellar origin. Two DIBs at 4428 and 5780 Å were found to be unusually strong in C₆₀-containing planetary nebulae (Díaz-Luis et al. 2015). These results strengthen the notion that there is a relationship between some DIB carriers and the fullerene-related compounds synthesized in circumstellar envelopes.

DIBs are likely to originate from molecules or radicals possessing strong oscillator strengths. Given the high stability of the carbon cage, C₆₀ is able to survive in rather harsh environments (see Cataldo et al. 2009, and references therein). The atomic and electronic structures of C₆₀ make it possible to form a great diversity of stable derivatives, including C₆₀H_m (fulleranes), C₆₀ adducts, X@C₆₀ (endofullerenes; X represents

one or more atoms or molecules), heterofullerenes, buckyons, and so on. This is consistent with the general property of DIBs because DIBs can be divided into different groups according to the correlations of intensities. The possibility of various fullerene compounds as the carriers of DIBs was recently discussed by Omont (2016).

In the laboratory, C_{60} can be readily hydrogenated into $C_{60}H_{36}$ by atomic hydrogen (see, e.g., Cataldo & Iglesias-Groth 2009; Iglesias-Groth et al. 2012). Since hydrogen is the most abundant element in the universe and fullerene has been discovered in H-rich circumstellar envelopes (García-Hernández et al. 2010), it is reasonable to expect that $C_{60}H_m$ might exist in space. Most of the experimental synthesis procedures of $C_{60}H_m$ are performed on condensed samples (Goldshleger & Moravsky 1997) and it is difficult to say whether the radiative association reaction of gas-phase C_{60} and H can efficiently produce $C_{60}H_m$. However, chemistry in astronomical environments can be quite different from that in laboratory and it is possible that circumstellar C_{60} exists in either or both solid-state and gas-phase forms (Zhang & Kwok 2013). Therefore, we cannot rule out the possibility that in space $C_{60}H_m$ can be formed on solid surfaces.

Experimental studies suggest that $C_{60}H_m$ would be quickly dehydrogenated to C_{60} in an inert gas atmosphere when the temperature approaches 550 K (Rüchardt et al. 1993). If astronomical fullerenes are free-flying gaseous species, temperatures well above 550 K can be readily reached through stochastic heating by absorption of a single UV photon. If this is the case, significantly hydrogenated fullerenes would presumably only be present in the environments which are rich in atomic H and devoid of UV radiation. While these two conditions have a relatively narrow intersection, they are satisfied by the circumstellar environment of reflection nebulae and proto-planetary nebulae.

Experimental data show that the C–H stretching bands of $C_{60}H_m$ at 3.4–3.6 μm have molar extinction coefficients similar to those of four major vibrational bands of C_{60} (Iglesias-Groth et al. 2012). These features were tentatively detected in the proto-planetary nebula IRAS 01005+7910, and the relative intensities suggest a large m value (Zhang & Kwok 2013). However, Díaz-Luis et al. (2016) did not detect fullerenes in two planetary nebulae exhibiting strong C_{60} emission, and concluded that they might have been destroyed by UV radiation. Indeed, the experimental study of Cataldo & Iglesias-Groth (2009) shows that molecular hydrogen can be released from $C_{60}H_m$ by UV radiation and the $C_{60}H_m/C_{60}$ abundance ratio depends on the equilibrium between the hydrogenation of C_{60} and the emission of molecular hydrogen.

Since spectral information on fullerenes from laboratory data is limited, it would be useful to perform theoretical studies to explore the vibrational signatures of $C_{60}H_m$. Recent advances in computational chemistry methods and computing facilities enable theoretical investigation of the vibrational properties of large molecules like fullerenes. In this paper, we present theoretical calculations of the infrared spectra of $C_{60}H_m$, which then are compared with observational data. Specifically, we investigate the effects of hydrogenation on the spectral behavior of C_{60} and whether the spectral signatures can be detected by astronomical observations.

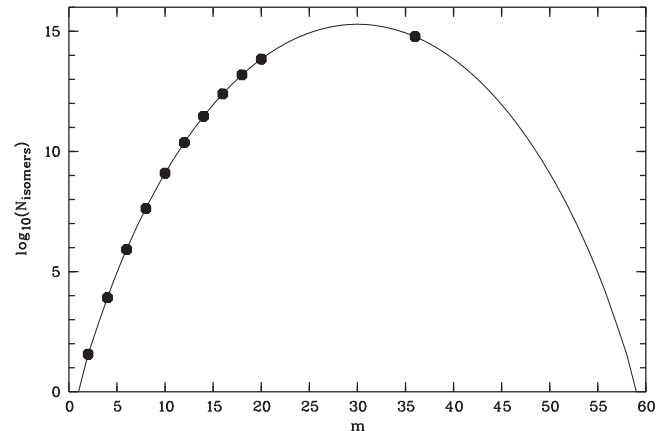


Figure 1. Number of $C_{60}H_m$ isomers with increasing m values. The filled circles mark the fullerenes considered in this paper.

2. $C_{60}H_m$ Isomers and Computational Methods

Under laboratory conditions, $C_{60}H_{36}$ is the most common product to be synthesized, though other fullerenes can also be produced. Thermal annealing can partly eliminate hydrogen from $C_{60}H_{36}$ to form $C_{60}H_{18}$ (Iglesias-Groth et al. 2012). The laboratory methods to synthesize fullerenes are summarized by Goldshleger & Moravsky (1997) and Cataldo & Iglesias-Groth (2010). Experimentally, C–H bonds are found to form through the addition of hydrogen across C = C double bonds, resulting in the numbers of hydrogen atoms in neutral fullerenes being always even. Guided by these experimental results, we have chosen to theoretically study 11 types of $C_{60}H_m$, where $m = 2, 4, \dots, 20$ and 36. Larger fullerenes ($m > 36$) are highly unstable due to significant structural strain.

Nevertheless, we cannot rule out the presence of fullerene radicals with odd hydrogen atoms in astronomical environments. In laboratory conditions where there are plenty of H atoms available, C_{60} is hydrogenated in the condensed phase, which is not necessarily the case in space. It is not unambiguously clear whether the dehydrogenation of fullerenes is accompanied by the release of H atoms or H_2 molecules. The calculations of Zerenturk & Berber (2012) show that the migration hydrogen on fullerenes have high barriers, unless the presence of a neighboring H atom lowers the migration barrier. If this is the case, the desorption of H_2 molecules would be more likely. Assuming that the formation route mimics the lab experiment, in which the most highly hydrogenated stable fullerene $C_{60}H_{36}$ is formed from C_{60} and then the lower hydrogenation species are created by losing H_2 , one will have only fullerenes with an even number of attached H atoms. Considering the relative difficulty of studying fullerenes with an odd number of H atoms (see below), it is desirable to begin with fullerenes with an even number of H atoms. Nevertheless, it would be useful to include fullerenes with an odd number of H atoms in future studies of association reactions of $C_{60}H_m$ with H atoms, dissociation paths, and their rates under space conditions.

Mathematically, the number of fullerene isomers can be obtained using a combinatorial approach. In Figure 1, we show the isomer numbers with increasing hydrogenation levels based on numbers in Table 2.5 of Bonchev & Rouvray (1995). As we can see from Figure 1, the number of structural isomers for

each $C_{60}H_m$ is enormous ($N \sim 10^{15}$ for $m = 30$). It would be computationally virtually impossible to explore all possible geometries. We therefore limit ourselves to study only five isomers for each species (except for $C_{60}H_{18}$, for which 20 isomers are included). While five is a very small fraction of the total isomer number, we note that the calculations of Bonchev & Rouvray (1995) do not take chemical stability into consideration. In the present calculations, we focus on those isomers that are likely to be the most stable, and an investigation of the effect of limited isomer numbers will follow in Section 3.3.

The initial geometries of the isomers were generated based on the most stable isomers reported in the experimental and theoretical works of Cataldo & Iglesias-Groth (2010). In general, we start from $C_{60}H_2$ isomer and hydrogen atoms were added sequentially to generate the other fullerenes isomers. The initial structures were visualized using the Chemcraft graphical program⁶ to avoid similar geometries among isomers. For highly hydrogenated C_{60} , H atoms are distributed as uniformly as possible over the C_{60} cage to minimize the effect of the repulsive forces between H atoms.

The computational procedures of $C_{60}H_m$ vibrational spectra are similar to those described in Sadjadi et al. (2015). Density functional theory (DFT) calculations were conducted with the Gaussian 09 (Frisch et al. 2009), PQS,⁷ and Firefly⁸ packages, running on the HKU supercomputer grid-point facility and QS128-2300C-OA16 QuantumCubeTM machine separately. We used the B3LYP and BH&HLYP hybrid functionals in combination with polarization consistent basis set PC1 (Jensen 2001, 2002) to obtain the harmonic frequencies of fundamental vibrations of the molecules. Under the default criteria, all the optimized geometries were characterized as local minima, established by the positive values of all harmonic frequencies and their associated eigenvalues of the second derivative matrix. Figure 2 shows the optimized structures of $C_{60}H_m$ isomers included in this study. The isomers are arranged from left to right in order of increasing relative total energy.

The scheme of double scaling factors (Laury et al. 2012) was then applied to the DFT vibrational frequencies. In this scheme, the vibrational frequencies of $>1000\text{ cm}^{-1}$ and $<1000\text{ cm}^{-1}$ are scaled by 0.9311 and 0.9352 for BH&HLYP and by 0.9654 and 0.9808 for B3LYP, respectively. In order to compare the computed absorption spectra with the observed emission spectra, we assumed a thermal excitation model at a temperature of 400 K, and applied a Drude broadening function to the theoretical spectra of $C_{60}H_m$ isomers. The width is assumed to be about $0.3\text{ }\mu\text{m}$, in accordance with the observed widths of C_{60} features. The assumed temperature is comparable to those determined from astronomical spectra. Finally, the theoretical spectrum of each $C_{60}H_m$ was obtained by averaging its five isomer spectra.

The accuracy of such a combination of DFT functionals, basis set, and scaling factors were estimated as $0.12\text{--}0.13\text{ }\mu\text{m}$ in reproducing experimental wavelengths (Sadjadi et al. 2015). The uncertainties of the band strengths are difficult to estimate. Inconsistent band strengths of C_{60} have been reported in the literature, and there are large discrepancies between the

theoretical and experimental values (see Zhang & Kwok 2013; Brieva et al. 2016, and references therein). Nevertheless, DFT has been evaluated as having an excellent performance in predicting the relative infrared intensities and Raman activities (Zvereva et al. 2011). From our calculations, we obtain the relative intrinsic strengths⁹ of the C_{60} bands at 18.9 , 17.4 , 8.5 , and $7.0\text{ }\mu\text{m}$ to be 100 , 37 , 31 , and 71 , lying well within the range of the previously reported values. The computed spectra of C_{60} are compared with the Fourier-transform infrared data from F. Cataldo (2017, private communication) in Figure 3. The reasonable agreement between theory and experiment gives us confidence in the theoretical results.

Modeling the electronic ground states of the open-shell systems such as fullerene radical cations via DFT formalisms requires additional efforts. In order to eliminate the spin contamination from the wave function occurring in unrestricted DFT formalism such as UB3LYP, we set our model to the restricted open-shell formalism. The second derivative energy matrix is calculated by numerical methods in the latter method rather than analytical methods in the former, which need more computational time. We tested the reliability of our chosen restricted open-shell approach in predicting the correct electronic structure by calculating the first ionization potential of C_{60} from the energy difference of C_{60} and C_{60}^+ . The geometry optimization and frequency calculations on C_{60}^+ were performed with ROB3LYP/PC1. The calculated ionization energy is 7.85 eV , which is in excellent agreement with the experimental value of $7.65 \pm 0.20\text{ eV}$ reported in Pogulay et al. (2004). Results of a limited study of cations are presented in Section 3.4.

3. Results

From Figure 2, we can see that the geometry of the carbon cages is distorted by sp^2 to sp^3 hybridization change of carbon atoms undergo hydrogenation in different parts of the C_{60} cage. In the classical view of interacting hard-sphere atoms, the repulsion between H atoms is expected to increase the strain energy in cage, which may cause the instability and further decomposition of very heavily hydrogenated C_{60} . As results of hydrogenation and rearrangement of π bonds, different kinds of C–C bonds such as conjugated, olefinic, and aromatic bonds are formed. The resultant breaking of the symmetry of C_{60} cage leads to the activation of more C–C modes and changes the relative strengths of the four skeletal vibrational bands of C_{60} , as well as forming new bands. The addition of H atoms to the C_{60} molecule is also expected to introduce new C–H stretching and bending modes, with corresponding increase in intensities with the number of H atoms. These effects will be quantitatively examined here.

3.1. The C–H Stretching Mode at $3.4\text{ }\mu\text{m}$

Figure 4 shows the calculated profiles of the C–H stretching bands near $3.4\text{ }\mu\text{m}$. These stretching modes result in multiple peaks ranging from 3.3 to $3.9\text{ }\mu\text{m}$, and there is a general tendency of increasing bandwidths with increasing m values. This may be attributed to the influence of neighboring environments of C–H groups. For a given C–H bond, the vibrational frequencies change depending on the number and distance of adjacent carbon atoms that are bonded to hydrogen (Webster 1992). When the m value is small, increasing

⁶ Available at <http://www.chemcraftprog.com>.

⁷ Parallel Quantum Solutions version 4.0, 2013 Green Acres Road, Fayetteville, Arkansas 72703; URL: <http://www.pqs-chem.com>.

⁸ Firefly version 8.2.0, <http://classic.chem.msu.edu/gran/firefly/index.html>.

⁹ In this paper, if not mentioning intrinsic strengths, all the band intensities or intensity ratios refer to those modeled.

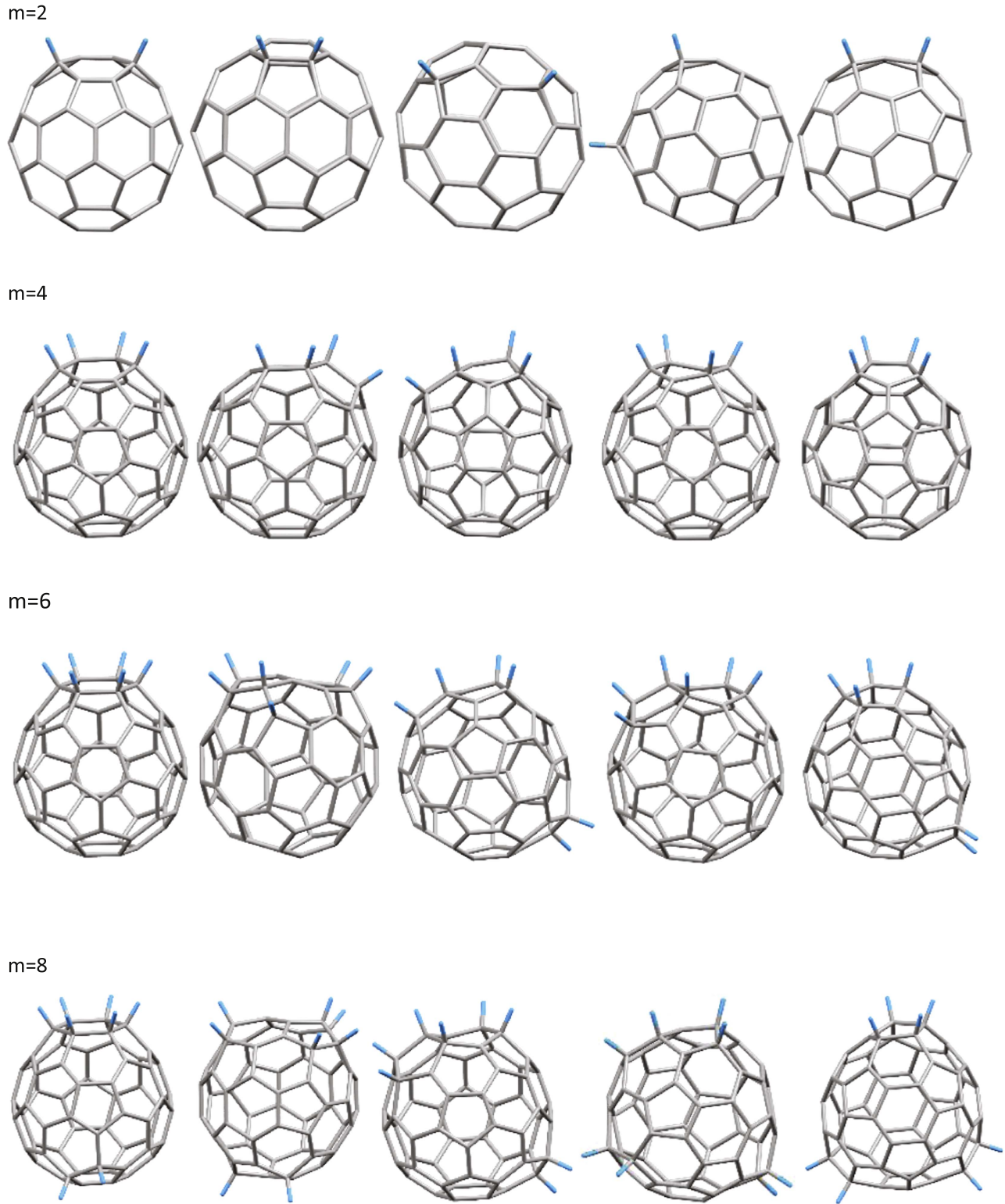
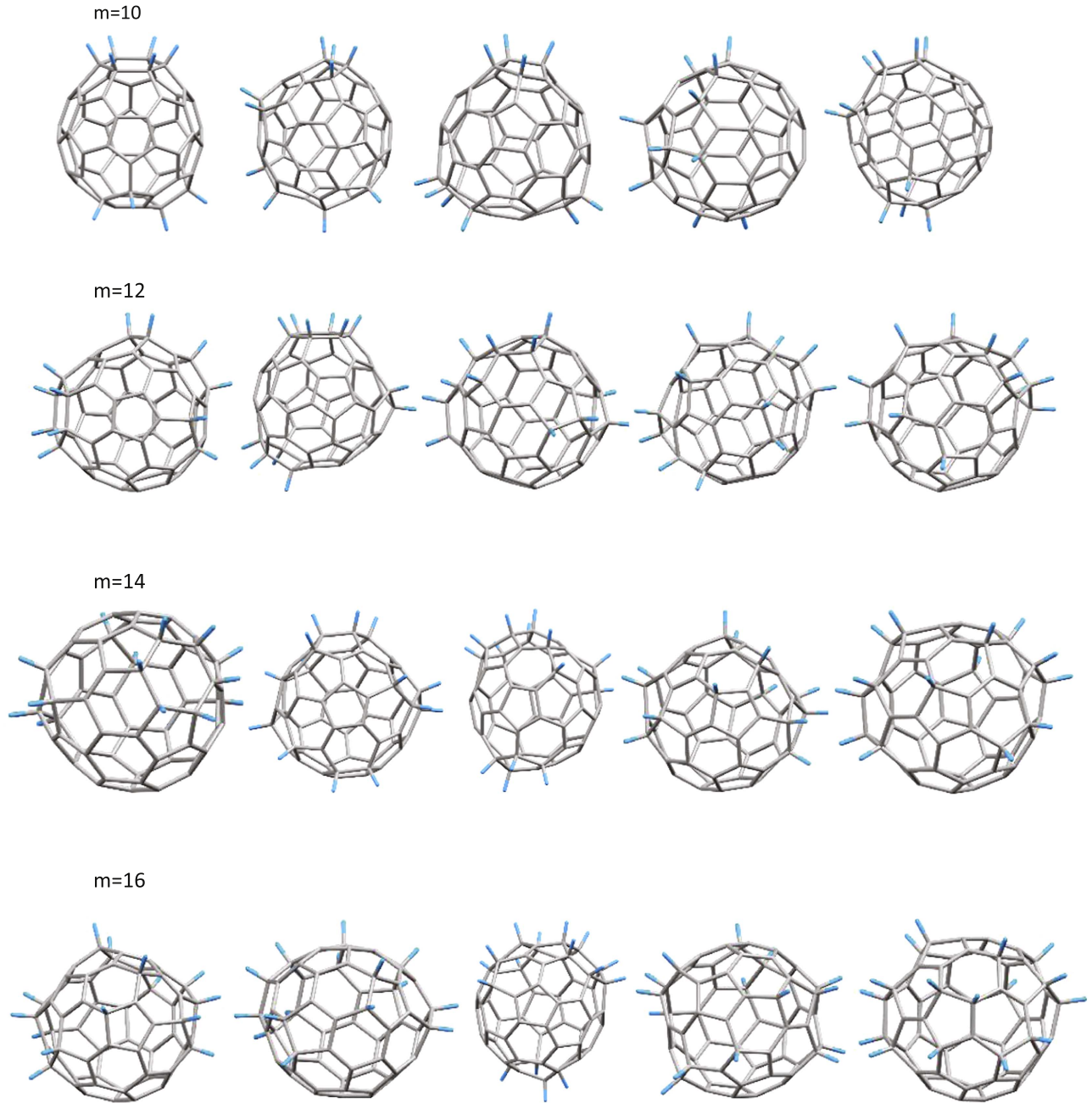


Figure 2. Local minimum geometries of $C_{60}H_m$ isomers from model calculations. A total of 55 structures, 5 isomers for each of $C_{60}H_m$, $m = 2, 4, 6, 8, 10, 12, 14, 16, 18, 20, 36$ are included in our study. The numbers of the isomers are assigned as 1 to 5 from left to right. The carbon cage is shown in gray and the C–H bonds are shown in blue. We can clearly see the geometric distortion of the C_{60} cage when hydrogen atoms are attached. The vibrational wavelengths and intrinsic strengths of these isomers are included as the data behind the figure.

hydrogenation leads to more complexity, and thus more complex band profiles. Beyond a certain m value, further hydrogenation results in lower numbers of vacant sites and decreases the complexity. Therefore, the $3.4 \mu\text{m}$ band profile is

a reflection of the symmetry of the molecule and can be taken as a probe of the structures of $C_{60}H_m$.

The $3.4 \mu\text{m}$ band arising from less symmetric $C_{60}H_m$ might be very broad and may be difficult to detect in astronomical

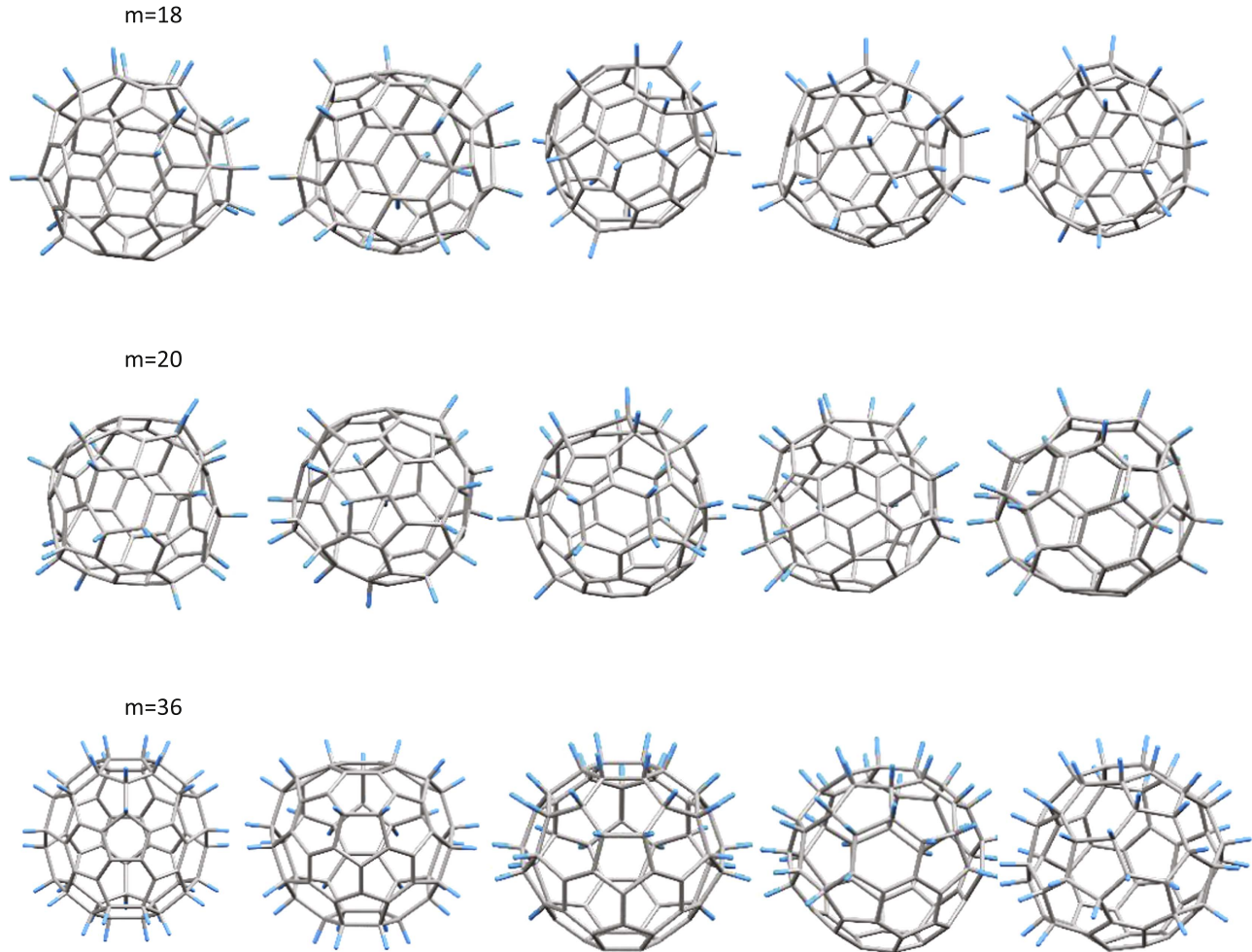
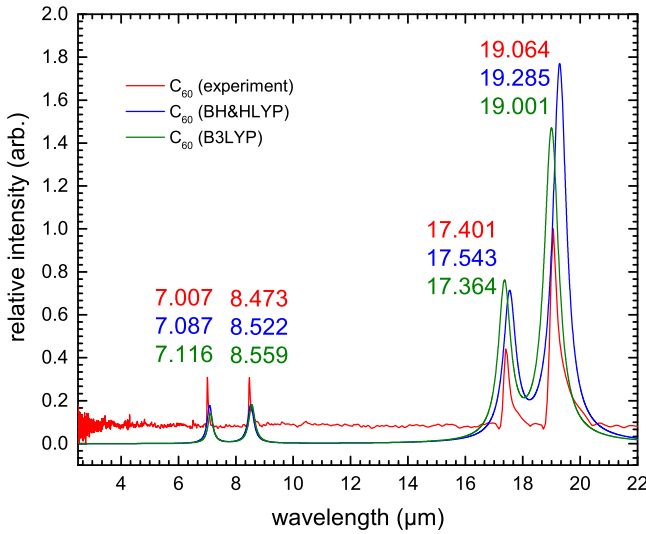
**Figure 2.** (Continued.)

spectra. A mixture of $C_{60}H_m$ isomers may produce a broad plateau around $3.4\ \mu\text{m}$, a feature that has been commonly observed in astronomical sources.

The strengths of the $3.4\ \mu\text{m}$ band are positively correlated with the degree of hydrogenation, as illustrated in Figure 4. If C_{60} is only slightly hydrogenated, the $3.4\ \mu\text{m}$ band may be too weak to be detectable in astronomical spectra. In Figure 5, we examine the variations of the intensities with the m values. A positive correlation can be seen, though the relation is clearly nonlinear. When $m \leq 20$, the band intensities per hydrogen atom increase with increasing m values. This shows that the C–H oscillators do not remain isolated from one another. The presence of additional H atoms affects the distribution of

electrons, which respond to the distortion along C–H stretches and yield larger variations of the electric dipole moment.

Experimental data suggest that the C–H stretching bands of $C_{60}H_{36}$ and $C_{60}H_{18}$ have molar extinction coefficients (normalized with the number of CH groups) larger than those of aliphatic molecules (Iglesias-Groth et al. 2012). Therefore, if fullerenes with high hydrogenation have an abundance comparable to aliphatic species, they should be easily detected in astronomical spectra through the $3.4\ \mu\text{m}$ band. Four bands around $3.4\ \mu\text{m}$ in the spectrum of IRAS 01005+7910 have been tentatively assigned to fullerenes, and their relative intensities might suggest that there exist species with different degrees of hydrogenation (Zhang & Kwok 2013). An

**Figure 2.** (Continued.)**Figure 3.** Theoretical spectra of C_{60} obtained using the B3LYP (green) and BH&HLYP (blue) functionals, compared with the experimental data (red) of F. Cataldo (2017, private communication). The peak wavelengths are indicated with the corresponding colors.

inspection of Figure 4 clearly suggests that it is possible to qualitatively reproduce the observed features by weighted sums of these computed spectra, while a quantitative comparison

between theoretical and observational spectra requires more extensive computations of $C_{60}H_m$ isomers.

Because $C_{60}H_m$ has a rather low ionization potential, $C_{60}H_m^+$ may be present in the diffuse interstellar medium and contribute to the DIB phenomenon. Theoretical computations and experimental data of polycyclic aromatic hydrocarbons (PAHs) show that the C–H stretching mode is greatly suppressed in cations (Pauzat et al. 1995). Topological analysis of Pauzat et al. (2010) shows that a hole in the π shell created by ionization may be responsible for the suppression of C–H modes in PAH cations. It is therefore worthwhile to investigate whether such a suppression also occurs for fullerenes. A detailed study of the vibrational spectrum of $C_{60}H_m^+$ is beyond the scope of this paper, but should be pursued in the future. A preliminary study of two ionized species of fullerenes is given in Section 3.4.

3.2. C–H Bending and Carbon Skeleton Motions in the 5–24 μm Spectral Region

Due to the intrinsic weakness in C–H stretching intensities of the fullerenes with low hydrogen content, the non-detection of the 3.4 μm in two C_{60} sources (Díaz-Luis et al. 2016) cannot be used to infer their absence, and the search should be focused on the spectral range at longer wavelengths. Figure 6 shows the theoretical spectra of C_{60} and $C_{60}H_m$ in the 5–24 μm region.

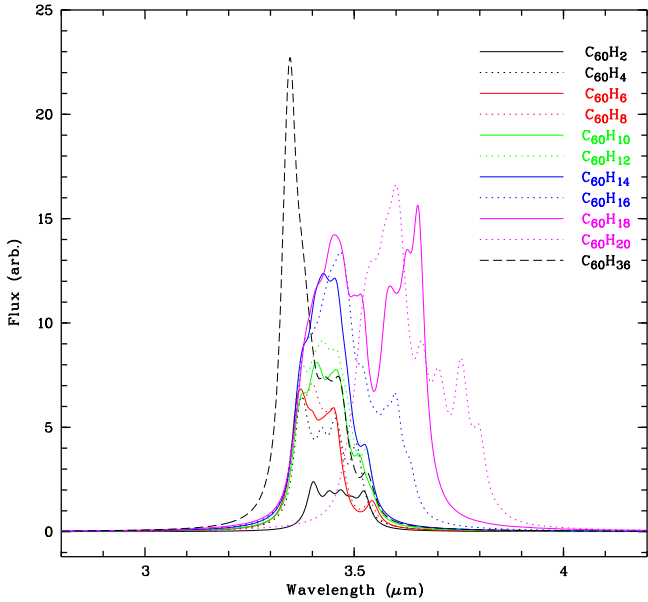


Figure 4. Theoretical profiles of the $C_{60}H_m$ $3.4\ \mu\text{m}$ feature. Each profile is the mean of five isomers.

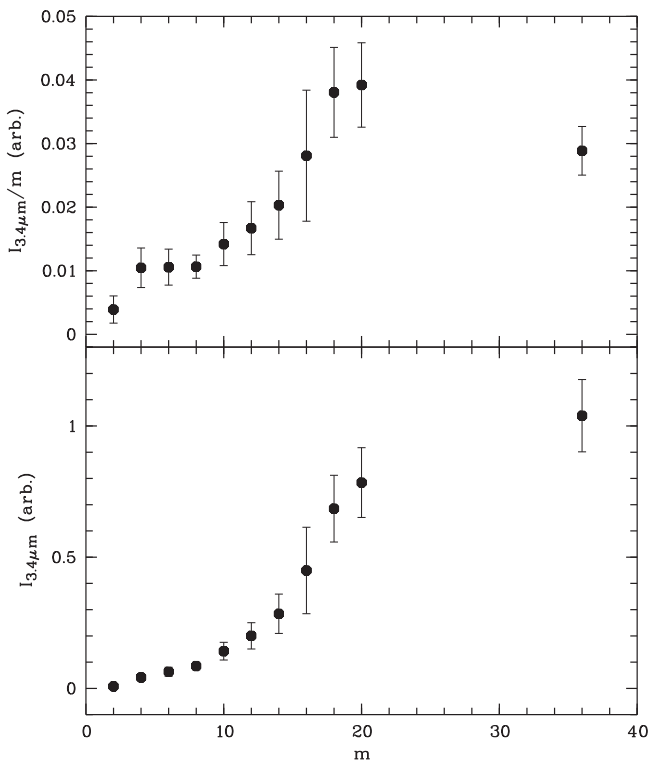


Figure 5. Intensities of the $3.4\ \mu\text{m}$ feature ($I_{3.4\mu\text{m}}$; lower panel) and $I_{3.4\mu\text{m}}/m$ (upper panel) vs. the m values of $C_{60}H_m$. The bars represent the standard deviations of the means of different isomers.

For comparison, we have also plotted the continuum-subtracted *Spitzer* spectrum of IRAS 01005+7910 (see Zhang & Kwok 2011, for details). Because of its high degree of symmetry, C_{60} has only 4 infrared-active and 10 Raman-active vibrational features. All the infrared-active bands, except the one badly blended with the Unidentified Infrared Emission (UIE) band at $8.6\ \mu\text{m}$, are clearly detected in IRAS 01005+7910. With

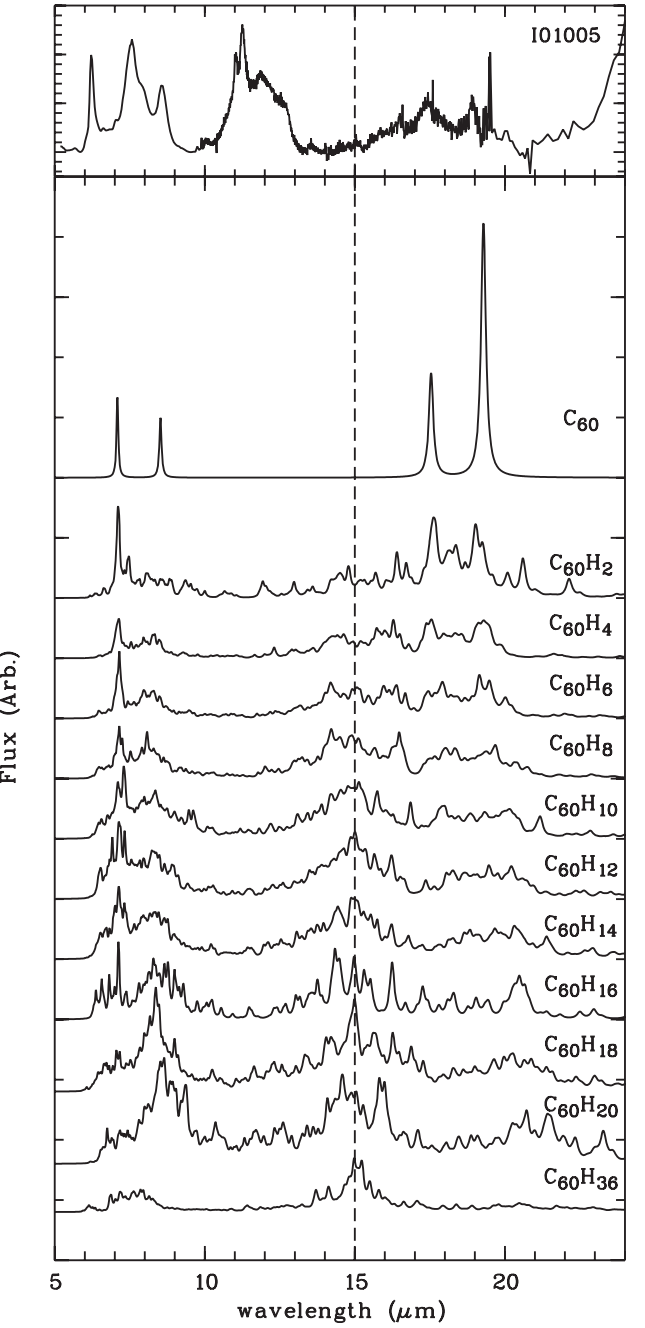


Figure 6. Spectrum of IRAS 01005+7910 (top panel) and theoretical spectra of C_{60} (second panel) and $C_{60}H_m$ (lower panels). The dashed line marks the position of the $15\ \mu\text{m}$ feature.

hydrogenation, the symmetry of the C_{60} backbone is broken, and thus some Raman-active modes become infrared-active. It is expected that C–H bending coupled with C_{60} skeletal vibrational modes could produce a large number of bands in this spectral region.

From Figure 6, we can see broad emission features around 8, 15, and $20\ \mu\text{m}$ in most of the fullerenes, which are qualitatively consistent with the experimental spectra of Iglesias-Groth et al. (2012). Indeed, these broad features are also present in the spectrum of IRAS 01005+7910. However, since plateau features, especially those at 8 and $12\ \mu\text{m}$, can also be manifestation of aliphatic C–H bending modes (Kwok et al. 2001) or the effects of

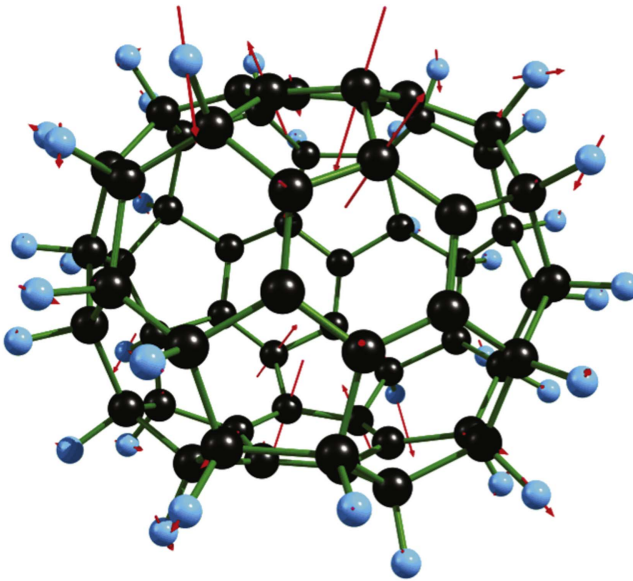


Figure 7. Vibrational mode of $C_{60}H_{36}$ responsible for the $15\ \mu m$ band. Black and blue circles represent carbon and hydrogen atoms, respectively. The C–C and C–H bonds are shown as green lines. The red arrows indicate the direction of relative motions. An animation of this vibration mode can be viewed in the online version of the paper.

(An animation of this figure is available.)

anharmonicity and Fermi resonance in hot ordinary PAH (see Maltseva et al. 2015, for a study of the plateau in the $3\ \mu m$ region), we cannot uniquely attribute the plateau features in IRAS 01005+7910 to $C_{60}H_m$. Below, we will discuss the origin of all three features.

The $8\ \mu m$ feature: vibrations around $8\ \mu m$ are generally due to C–H bending modes, along directions parallel to the tangential plane of the carbon sphere. A broad $6\text{--}9\ \mu m$ feature is generally apparent in the spectra of fullerene-rich planetary nebulae in the Magellanic Clouds (García-Hernández et al. 2012), which seems to resemble the theoretical spectra of fullerenes.

The $15\ \mu m$ feature: this feature arises from the breathing mode (sometimes referred to as the radial mode) of carbon atoms where the skeleton inflates and deflates, coupled with peripheral C–H bending motion. A schematic illustration of this mode for $C_{60}H_{36}$ is shown in Figure 7.

The $20\ \mu m$ feature: vibrational modes in the $20\ \mu m$ region are generally carbon skeleton deformation modes, where the angular and length separations between carbon atoms change with vibration. There is a well-known unidentified broad emission feature—known in the literature as the $21\ \mu m$ feature—in this region (Kwok et al. 1989). The feature has been attributed to fullerenes by Webster (1995) based on force-field and elastic-shell models. Our calculations show that fullerenes can indeed produce broad features spanning the wavelength range $17\text{--}23\ \mu m$. However, the profiles and peak positions of fullerenes vary greatly from one species to another, in contrast to the consistent peak wavelength and feature profiles of the observed $21\ \mu m$ feature (Volk et al. 1999). We are unable to reproduce the observed $21\ \mu m$ feature profiles with one, or the sum of more, theoretical fullerene spectra. This, together with the fact that there is no correlation between

the $21\ \mu m$ feature and C_{60} (Zhang et al. 2010; Zhang & Kwok 2011), lead us to conclude that fullerenes are not carriers of the $21\ \mu m$ feature.

3.3. Spectral Variation among Isomers of $C_{60}H_{18}$

In order to assess the degree of spectral variation in different fullerene isomers, we have expanded the number of isomers from 5 to 20 for $C_{60}H_{18}$ (Figure 8). The relative energy values of these 20 isomers expand to a range of 80 kcal/mol (corrected for zero point energy). Together with direct comparison of molecular geometry parameters, this ensures the acceptable structural diversity of among these isomers. The theoretical spectra of these 20 isomers are shown in Figure 9. Also plotted is the area (shown in gray) covered by one standard deviation of the 20 spectra. All four dominant features around $3, 8, 15$, and $20\ \mu m$ are present, regardless of the variation in m values. These results suggest that the existence of the features is not specific to a particular isomer. Specifically, the broad feature around $8\ \mu m$ is the strongest one, followed by the feature that peaks around $15\ \mu m$. Unlike the $15\ \mu m$ feature, the features around $20\ \mu m$ vary greatly in intensities and peak positions among the isomers. The intensities of the $3.4\ \mu m$ feature are not sensitive to the specific isomer.

3.4. Spectra of Fullerene Cations

In order to test the possible effect of ionization on the spectral behavior of fullerenes, we have computed the spectra of two ionized species with low and high degrees of hydrogenation: $C_{60}H_2^+$ and $C_{60}H_{36}^+$ starting from the geometries of their lowest energy neutral isomers (isomer1). It is well known that due to theoretical limitations in dealing with the electronic energy states close to the ground one that arise in fullerenes and fullerenes when they have an open-shell electronic structure, the wavelengths and intensities of the C–C vibrations are not accurate (Pauzat 2011). Consequently, we focus only on the C–H stretching bands in the $3\text{--}4\ \mu m$ wavelength range. From results of DFT calculations, we obtain co-added intensities of $8.4305, 21.0465, 1265.5103$, and $533.8743\ km\ mol^{-1}$ for the $3\text{--}4\ \mu m$ features of $C_{60}H_2$, $C_{60}H_2^+$, $C_{60}H_{36}$, and $C_{60}H_{36}^+$, respectively. The theoretical spectra of these molecules are shown in Figure 10. We can see from the figure that the peak positions and profiles appear to be invariant between neutral and ionized fullerenes, which could be attributed to the same geometries and symmetries. However, the change in intensity of the $3\text{--}4\ \mu m$ features upon ionization is not simple. $C_{60}H_{36}^+$ shows a decrease in intensity of its C–H stretching bands, while the opposite is true for $C_{60}H_2^+$. Such a spectral behavior is different from that of PAH molecules where the C–H stretching modes are suppressed in ions. Such suppression is not a direct result of ionization, but rather the result of changes of electronic structures upon ionization (Pauzat et al. 2010). Specifically, band intensities reflect the distortion of electronic density with internal displacements of the nuclei. More thorough studies of fullerene cations are required to determine the effects of ionization and how such changes depend on specific isomers and hydrogen contents.

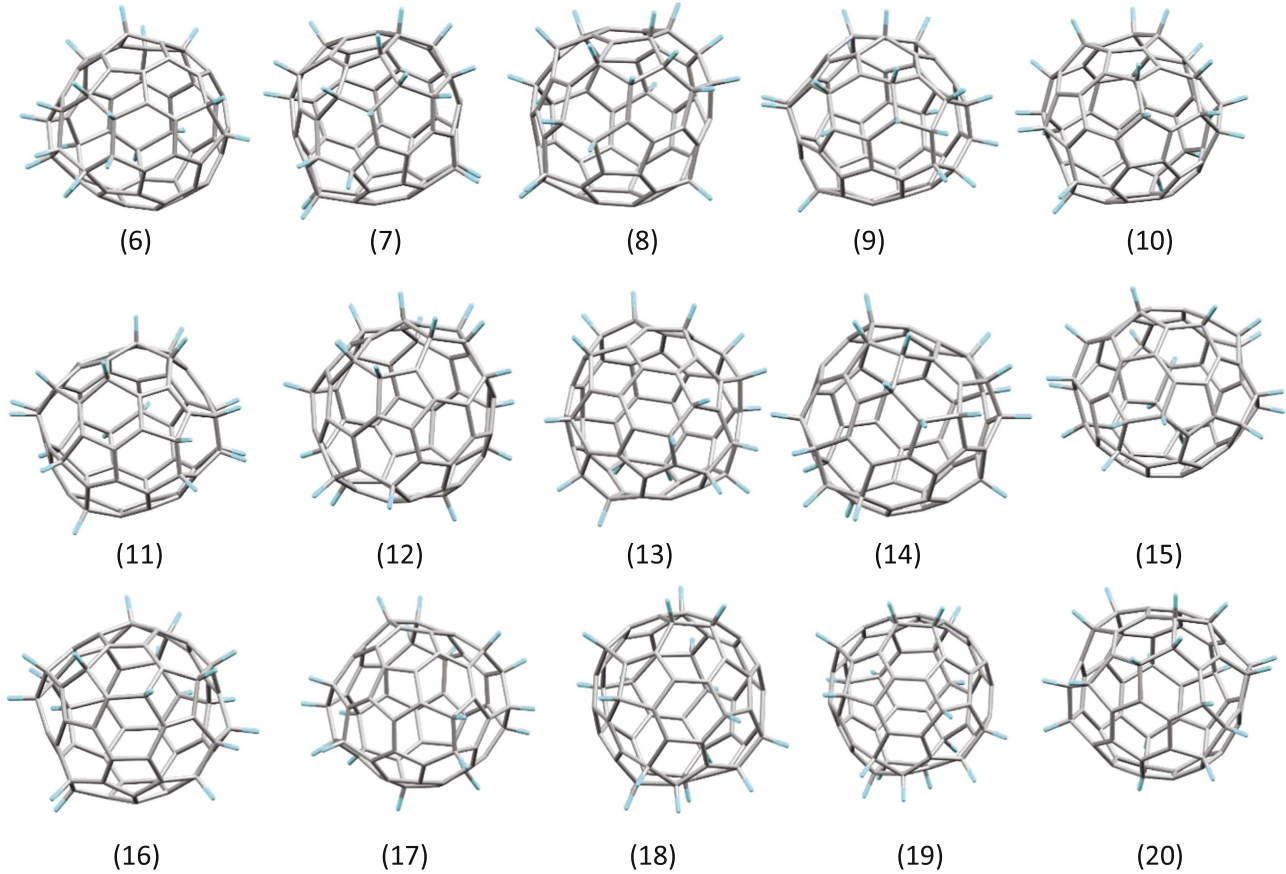


Figure 8. Geometry of 15 additional isomers of $C_{60}H_{18}$. The numbers in brackets indicate the isomer numbers. The vibrational wavelengths and intrinsic strengths of the isomers are provided as the data behind the figure.

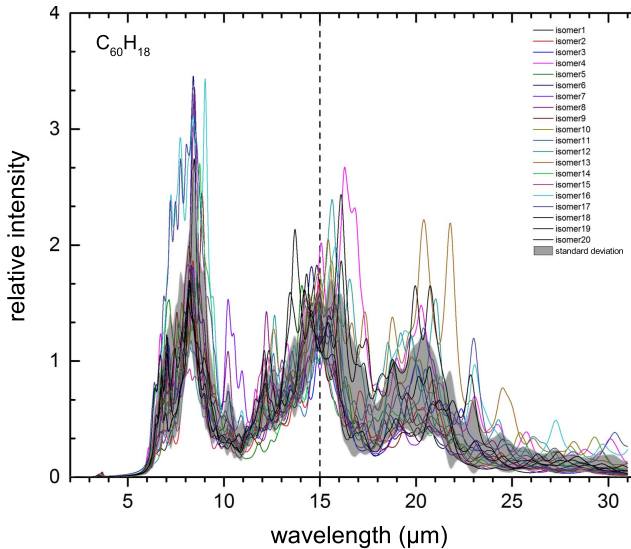


Figure 9. Spectral variation of 20 isomers of $C_{60}H_{18}$. The isomer numbers in the legend are those given in Figures 2 and 8. The vertical dashed line marks the position of the $15\ \mu m$ feature. The gray area represents the area covered by one standard deviation from the 20 spectra.

4. Discussions

4.1. Origin of the Scatter of Observed Band Ratios in C_{60} Sources

The fullerene (C_{60}) molecule was detected through their four infrared-active bands due to carbon skeletal modes. These four

bands are still visible for slightly hydrogenated C_{60} , but gradually fade with increasing hydrogenation (Figure 6). It is therefore possible that the astronomical C_{60} bands reported in the literature could actually arise in part from slightly hydrogenated C_{60} . This suggests that C_{60} and its hydrogenated derivatives may be more prevalent than previously believed because progressive hydrogenation would make the four infrared bands more difficult to detect.

In Figure 11, we quantitatively compare the variations of the intrinsic strengths of the four bands as functions of the m values. It is shown that the total intrinsic strengths decrease with increasing hydrogenation, and the intrinsic strengths of individual bands have different m dependencies. The bands at longer wavelengths appear to weaken more rapidly compared to the $7.0\ \mu m$ feature. With increasing hydrogenation, the intensity of the $7.0\ \mu m$ band decreases by a factor of about 1.5 and then remains nearly constant until $m > 14$, while the intensities of the 18.9 and $17.4\ \mu m$ bands continually decrease by more than one order of magnitude. Therefore, the relative strengths of the four skeletal bands are different for C_{60} and $C_{60}H_m$.

The observed relative strengths of the four C_{60} bands have been used to infer excitation mechanisms of the molecule (Bernard-Salas et al. 2012; García-Hernández et al. 2012; Roberts et al. 2012; Zhang & Kwok 2013). However, it is difficult to distinguish between fluorescence and thermal excitation mechanisms because of the uncertainties in the intrinsic band strengths. This problem was recently re-examined by Brieva et al. (2016), who presented new

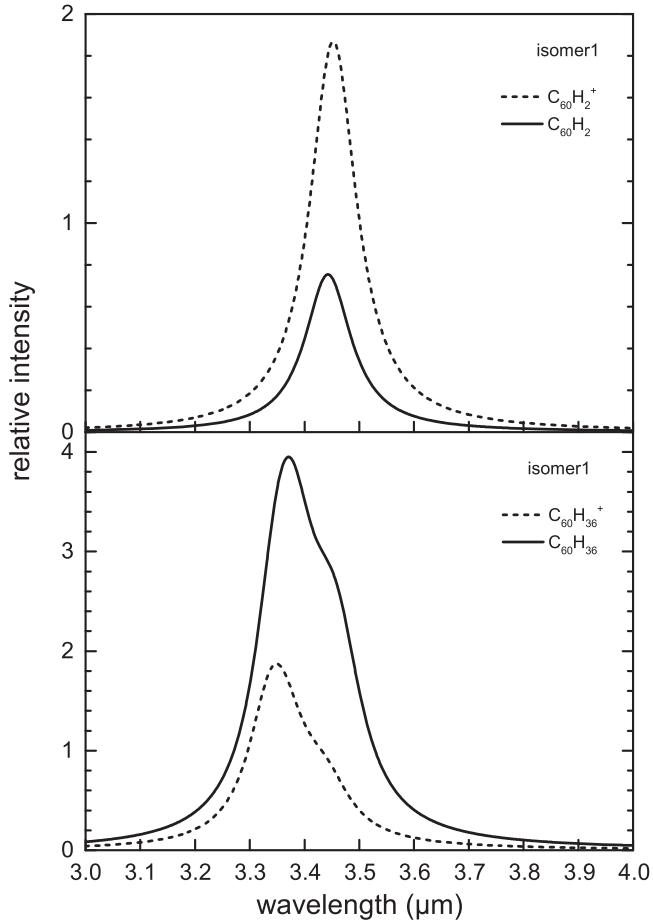


Figure 10. Theoretical spectra of two fullerene cations in the $3\text{--}4\,\mu\text{m}$ region. The upper panel shows the comparison between the spectra of $C_{60}H_2$ (solid line) and $C_{60}H_2^+$ (dashed line) and the lower panel between $C_{60}H_{36}$ (solid line) and $C_{60}H_{36}^+$ (dashed line).

laboratory measurements of the intrinsic strengths. Even using the latest data, the observed band ratios are too dispersed to be assigned to either fluorescence or thermal excitation models. Brieva et al. (2016) attributed this inconsistency to contamination of the band strengths from UIE or other emissions, which if true would severely limit the utility of C_{60} infrared bands as a probe of physical conditions in circumstellar environments.

In Figure 12, we investigate the possibility of whether the hydrogenation of C_{60} may play a role in the wide scatter of the observed band ratios. The observed band ratios are taken from Bernard-Salas et al. (2012), García-Hernández et al. (2012), and Otsuka et al. (2014). We should note that even for the strong C_{60} -source Tc 1, different authors report different $7.0\,\mu\text{m}/8.5\,\mu\text{m}$ band ratios partly due to different ways of subtracting other line contributions. The variation of the band ratios as a function of temperature under the thermal excitation model is plotted. We note that the predicted band ratios by the fluorescence model are very close to those by the thermal model (Brieva et al. 2016). Figure 12 shows that the large scatter of the observed $17.4\,\mu\text{m}/18.9\,\mu\text{m}$ band ratios cannot be accounted for by the model characterized by the single parameter (i.e., average photon energy and temperature for fluorescence and thermal model, respectively). However, the inconsistency can be explained by hydrogenation effects. First,

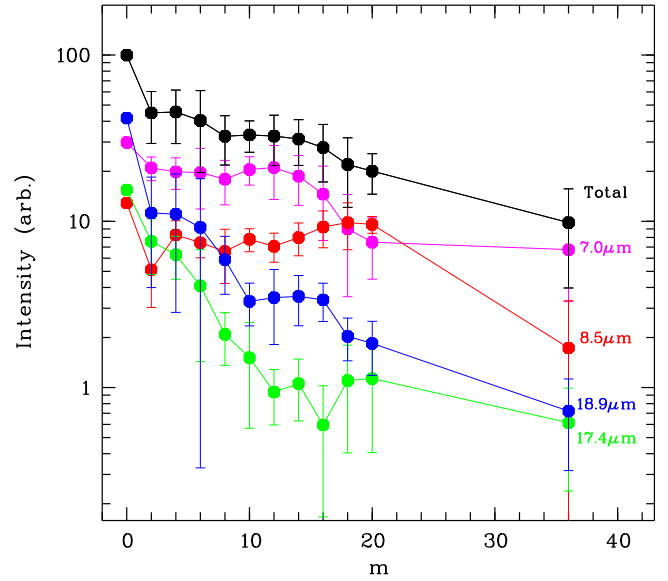


Figure 11. Intrinsic strengths of the four carbon skeletal vibration modes (7.0 , 8.5 , 17.4 , and $18.9\,\mu\text{m}$) vs. the m values of $C_{60}H_m$. The black curve represents the total of the four bands. The error bars represent the standard deviations of the means of different isomers.

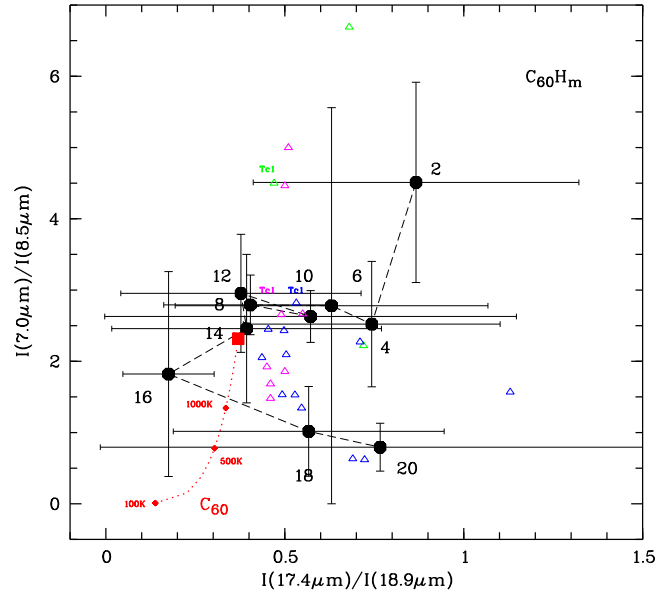


Figure 12. Intrinsic strength ratios of $C_{60}H_m$ (filled circles connected by dashed line), where the bars represent the standard deviations of the means of different isomers. The marked numbers represent the m value. The red square marks the position for C_{60} . The dotted curve represents the predicted ratios for a thermal excitation of C_{60} . The green, blue, and magenta open triangles are the observed values taken from Bernard-Salas et al. (2012), García-Hernández et al. (2012), and Otsuka et al. (2014), respectively. For the sake of clarity, the error bars of the observed values are not plotted.

different hydrogenation degrees and diverse isomers of $C_{60}H_m$ can contribute to the scatter of the observed band ratios. Second, most of $C_{60}H_m$ show larger theoretical $17.4\,\mu\text{m}/18.9\,\mu\text{m}$ band ratios than C_{60} . The fact that the observed data lie within the range covered by the theoretical values of $C_{60}H_m$ in Figure 12 suggests that hydrogenated C_{60} may be present in these sources and contribute to the observed infrared bands.

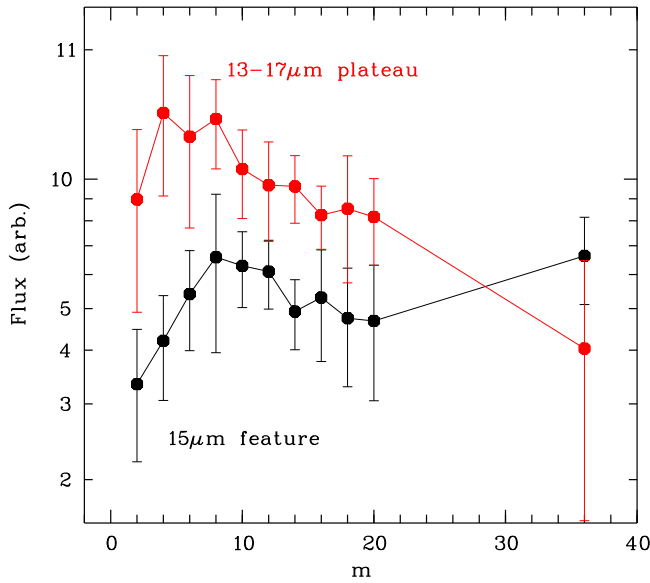


Figure 13. Fluxes of the $15\text{ }\mu\text{m}$ feature (black) and the $13\text{--}17\text{ }\mu\text{m}$ plateau (red) vs. the m values of C_{60}H_m . The bars represent the standard deviations of the means of different isomers.

4.2. Search for Circumstellar C_{60}H_m

One of the major challenges in searching for circumstellar C_{60}H_m is the large number of isomers. Although $\text{C}_{60}\text{H}_{36}$ and $\text{C}_{60}\text{H}_{18}$ are the dominant products of the experiments of C_{60} exposed to hydrogen atoms, the physical conditions of circumstellar envelopes are very different from those in a terrestrial laboratory. Given the very low densities in circumstellar envelopes, the less stable fullerenes are likely to be present. Through averaging the theoretical spectra of different isomers (Figure 6), the bands that are commonly present in all the isomers can serve as guides for the search of circumstellar C_{60}H_m . One of the distinctive features of the fullerene spectra is the emergence of a $13\text{--}17\text{ }\mu\text{m}$ plateau (Figure 6). As the number of H atoms increases, a band at $15\text{ }\mu\text{m}$ becomes more prominent. The variation of strengths of the $15\text{ }\mu\text{m}$ and the $13\text{--}17\text{ }\mu\text{m}$ plateau features with the m values are illustrated in Figures 13 and 14. We can see that the plateau feature is generally stronger than the $15\text{ }\mu\text{m}$ band except for $\text{C}_{60}\text{H}_{36}$. For heavily hydrogenated C_{60} , the $15\text{ }\mu\text{m}$ band clearly stands out from the plateau.

The $15\text{ }\mu\text{m}$ feature is unique to fullerenes. There is no known aromatic molecules having strong bands at $15\text{ }\mu\text{m}$. The bending modes of aliphatic compounds are concentrated around 8 and $12\text{ }\mu\text{m}$. CO_2 has a band at this wavelength, but it is not expected in carbon-rich environments. Thus the $15\text{ }\mu\text{m}$ band might serve as a useful probe of heavily hydrogenated C_{60} in circumstellar envelopes.

We have undertaken a search for the $15\text{ }\mu\text{m}$ band in known C_{60} sources (Appendix A). The exact positions of the vibrational bands in theoretical spectra are affected by the scaling factor applied (Section 2) and this is evident in the slight wavelength differences seen in the theoretical and experimental wavelengths spectra of C_{60} (Figure 3). Consequently, we cannot take the peak wavelength of $15\text{ }\mu\text{m}$ as the definitive signature of fullerene. Nevertheless, we note that several objects display features with wavelengths close to $15\text{ }\mu\text{m}$. Three C_{60} -containing objects (IRAS 01005+7910, IRAS 06338+5333, NGC 7023) display

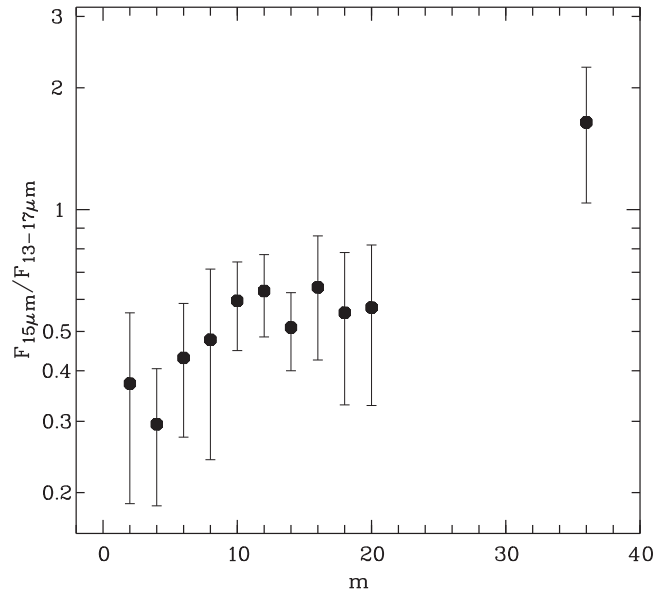


Figure 14. Flux ratios between the $15\text{ }\mu\text{m}$ feature and the $13\text{--}17\text{ }\mu\text{m}$ plateau vs. the m values of C_{60}H_m . The bars represent the standard deviations of the means of different isomers.

a feature at $15\text{ }\mu\text{m}$.¹⁰ We note that none of these three objects have a hot central star, which is consistent with the suggestion of Díaz-Luis et al. (2016) that fullerenes are quickly destroyed by increasing UV radiation. Given the weakness of the features, we must regard the detections in the three sources as tentative.

Since hydrogenation can greatly suppress the four C_{60} skeletal bands, the search for fullerene should not be limited to sources showing the four C_{60} bands. A more extensive search for the $15\text{ }\mu\text{m}$ band should be conducted for a wider range of objects.

In the case of NGC 7023, spatially resolved spectra are available (Appendix B). Figure 15 shows five spectra of NGC 7023, from closest to the central star (“S1,” top panel) to farthest from the central star (“S5,” bottom panel). We can see that the $15\text{ }\mu\text{m}$ feature appears in positions “S3” and “S4,” where the C_{60} emission is becoming weak and H_2 emission is appearing. Sellgren et al. (2010) have shown that, compared to H_2 emission, the $18.9\text{ }\mu\text{m}$ C_{60} feature lies closer to the central star where UV radiation is more intense, while the UIE bands peak between the C_{60} and H_2 emission. Figure 15 indicates that the $15\text{ }\mu\text{m}$ feature and UIE are roughly co-spatial, supporting the idea that the preferential conditions for the presence of fullerenes are H atom rich and void of intense UV radiation. The observed feature is relative narrow, suggesting that C_{60}H_m isomers, if they exist, are not very diverse, and the physical conditions favor the formation of specific chemical structures.

We note that Berné et al. (2013) detected C_{60}^+ in the spectrum at $7.5''$ northwest from the central star of NGC 7023 (position 2 of their Figure 1). Figure 16 shows that the C_{60}^+ , C_{60} , UIE, and H_2 emission regions are spatially segregated in NGC 7023, suggesting that photochemistry plays a role in the formation of fullerenes. In the hypothesis of PAH being the carrier of UIE bands, fullerenes are formed in a top-down process where large

¹⁰ We note that the $8.5\text{ }\mu\text{m}$ features in the three sources are badly blended with the $8.6\text{ }\mu\text{m}$ UIE band and the $7.0\text{ }\mu\text{m}$ features are also blended with $\text{H}_2\text{S}(5)$ at $6.91\text{ }\mu\text{m}$ line (Werner et al. 2004) and thus the three sources are not included in Figure 12.

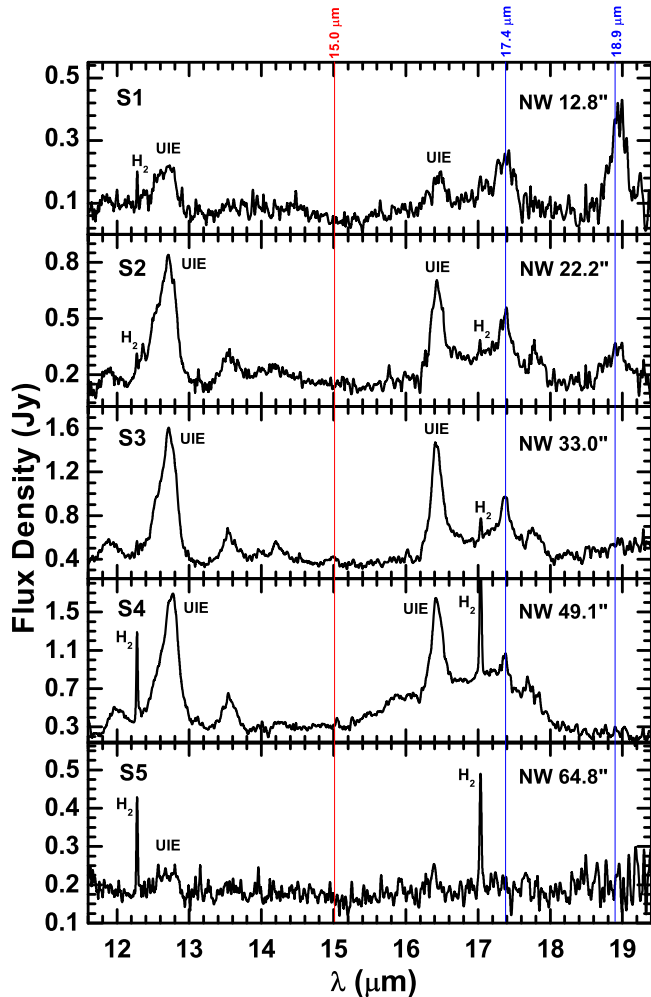


Figure 15. Five *Spitzer*-IRS SH continuum-subtracted spectra for NGC 7023 at various distances from the central star. The blue and red vertical lines indicate the positions of the C_{60} bands and $15.0\ \mu m$ features, respectively. Note that the $17.4\ \mu m$ C_{60} feature may be blended with a UIE band. The panel for each spectrum S1–S5 is labeled with the slit offset to central source in the unit of arcseconds. Two H_2 lines at 12.28 and $17.03\ \mu m$ are also marked.

PAHs are dehydrogenated by UV radiation, followed by carbon atom ejection and isomerization (Berné & Tielens 2012). If our detection and identification of the $15\ \mu m$ feature is correct, this scenario is contradicted by our observations of the $15\ \mu m$ fullerene feature being coincident with the distribution of the UIE bands. Alternatively, fullerenes/fulleranes are formed by the photochemical effects on mixed amorphous aromatic/aliphatic compounds (García-Hernández et al. 2010; Micelotta et al. 2012; Zhang & Kwok 2013). More theoretical work is needed to further pursue this idea.

5. Summary

Fulleranes are potentially important constituents of the interstellar medium for their possible role in the formation of molecular hydrogen and their relationships to the carriers of the UIE and DIB phenomena (Cataldo & Iglesias-Groth 2010). There are also strong theoretical and experimental reasons to believe that fulleranes are widely present in the circumstellar and interstellar environments. However, the search for circumstellar fulleranes has so far been hindered by the lack

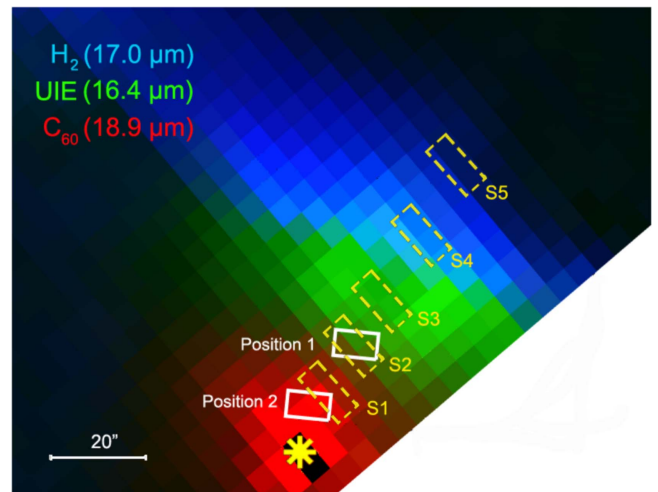


Figure 16. *Spitzer* composite-color image of NGC 7023 nebula based on Figure 1 in Berné et al. (2013), constructed from components of IRS low-resolution (LL) module spectral cube. The image was mainly made from three integrated band intensities: H_2 line at $17.0\ \mu m$ (shown in blue), the UIE band at $16.4\ \mu m$ (green), and C_{60} band at $18.9\ \mu m$ (red). North is up and east is to the left. The white rectangles indicate the positions where Berné et al. (2013) extracted their spectra. The yellow dashed rectangles represent the regions where the IRS-SH spectra (shown in Figure 15) have been extracted. The position of the central star is also marked with a yellow asterisk.

of detailed knowledge of their spectra. In this paper, we performed a theoretical investigation of the vibrational spectra of fulleranes using quantum chemistry methods. The results show that hydrogenation can have a significant effect on the determinations of the abundance and excitation mechanism of C_{60} . The inconsistent C_{60} band ratios between observations and model predictions might be an indirect proof for the existence of slightly hydrogenated C_{60} .

A feature at $3.4\ \mu m$ due to C–H stretching modes is generally present in the spectra of all fulleranes. Also noticeable are broad features around 8 , 15 , and $20\ \mu m$, which arise from C–H bending modes, carbon skeleton radial modes, and carbon skeleton deformation modes, respectively. The strength of the $15\ \mu m$ increases with increasing hydrogenation might possibly be a tracer of fulleranes. A spectral search suggests that this feature is present in three C_{60} -containing nebulae with no strong UV radiation background.

One of the major challenges in the study of astronomical fulleranes is the large (up to 10^{15} as shown in Figure 1) number of isomers, making theoretical calculations on all isomers impossible. In this paper, we have limited our study to isomers of lowest energies. Our results show definite spectral trends with progressive hydrogenation. The astronomical implications on the C_{60} skeletal bands are therefore likely to be independent on the selection of specific isomers. We plan to extend our computation to more fulleranes including different numbers of carbon and hydrogen atoms as well as different bond arrangements.

We gratefully acknowledge Franco Cataldo for providing us with their experimental spectra of fullerene. We also thank an anonymous referee and Anibal García-Hernández for helpful comments. This work makes use of observations made with the *Spitzer Space Telescope*, which is operated by the Jet Propulsion Laboratory, California Institute of Technology,

Table 1
The 15 μm Feature in C₆₀ Sources

Name	Instrument	15.0 μm	Class ^a	Object Type	References
2MASS J06314796+0419381	<i>Spitzer</i> IRS	...	M	YSO	(1)
DY Cen	<i>Spitzer</i> IRS	...	C	RCB	(2)
HD 52961	<i>Spitzer</i> IRS	: ^b	M	PAGB	(3)
HD 97300	<i>Spitzer</i> IRS	...	C	HAe/Be	(1)
Hen 2–68	<i>Spitzer</i> IRS	: ^c	C	PN	(4)
HR 4049	<i>ISO</i> SWS	: ^b	M	PAGB	(1)
IC 418	<i>ISO</i> SWS	: ^c	C	PN	(4)
IRAS 01005+7910	<i>Spitzer</i> IRS	\checkmark ^d	C	PPN	(5)
IRAS 06338+5333	<i>Spitzer</i> IRS	\checkmark ^d	M	PAGB	(3)
ISOGAL-P J174639.6-284126	<i>Spitzer</i> IRS	: ^e	M	YSO	(1)
K 3–54	<i>Spitzer</i> IRS	...	C	PN	(6)
K 3–62	<i>Spitzer</i> IRS	...	C	PN	(4)
Lin 49	<i>Spitzer</i> IRS	...	C	PN	(7)
LMC 02	<i>Spitzer</i> IRS	...	C	PN	(6)
LMC 25	<i>Spitzer</i> IRS	...	C	PN	(6)
LMC 48	<i>Spitzer</i> IRS	...	C	PN	(6)
LMC 99	<i>Spitzer</i> IRS	...	C	PN	(6)
M 1–6	<i>Spitzer</i> IRS	...	C	PN	(4)
M 1–9	<i>Spitzer</i> IRS	...	C	PN	(4)
M 1–11	<i>Spitzer</i> IRS	: ^d	C	PN	(4)
M 1–12	<i>Spitzer</i> IRS	...	C	PN	(4)
M 1–20	<i>Spitzer</i> IRS	...	C	PN	(4)
M 1–60	<i>Spitzer</i> IRS	...	C	PN	(6)
NGC 7023	<i>ISO</i> SWS	\checkmark ^d	C	RN	(8)
	<i>Spitzer</i> IRS	\checkmark ^d	C	RN	(8)
SaSt 2–3	<i>Spitzer</i> IRS	...	C	PN	(4)
SMC 13	<i>Spitzer</i> IRS	...	C	PN	(6)
SMC 15	<i>Spitzer</i> IRS	...	C	PN	(6)
SMC 16	<i>Spitzer</i> IRS	...	C	PN	(6)
SMC 18	<i>Spitzer</i> IRS	...	C	PN	(6)
SMC 20	<i>Spitzer</i> IRS	...	C	PN	(6)
SMC 24	<i>Spitzer</i> IRS	...	C	PN	(6)
SMC 27	<i>Spitzer</i> IRS	...	C	PN	(6)
SSTGC 372630	<i>Spitzer</i> IRS	...	M	YSO	(1)
Tc 1	<i>Spitzer</i> IRS	: ^c	C	PN	(9)
XX Oph	<i>Spitzer</i> IRS	...	M	Binary	(10)

Notes.^a M: mixed-chemistry dust, C: carbon-rich dust.^b A strong peak at 14.95 μm and two weak ones at about 15.05 and 15.1 μm .^c An extreme weak peak around 15.1 μm .^d A weak but still visible peak at 15.0 μm .^e A visible peak at 14.9 μm .

References. (1) Roberts et al. (2012), (2) García-Hernández et al. (2011), (3) Gielen et al. (2011), (4) Otsuka et al. (2014), (5) Zhang & Kwok (2011), (6) García-Hernández et al. (2012), (7) Otsuka et al. (2016), (8) Sellgren et al. (2010), (9) Cami et al. (2010), (10) Evans et al. (2012).

under a contract with NASA. Financial support for this work was provided by the Research Grants Council of Hong Kong under grants HKU 7027/11P and HKU7062/13P.

Appendix A

A Search for the 15 μm Feature in C₆₀ Sources

We examined the infrared spectra of 35 sources that have been reported to contain C₆₀ emission to search for the fullerene 15 μm feature. The C₆₀ source list (Table 1) includes young stellar objects (YSOs), Herbig Ae/Be star (HAe/Be), planetary nebulae (PNs), post-asymptotic giant branch stars (PAGBs), proto-planetary nebula (PPN), R Coronae Borealis star (RCB), binary, and reflection nebula (RN). The objects are

classified as carbon-rich (C) or mixed chemistry (M) (column 4 of Table 1) based on other spectral features in the infrared spectra. The spectra were extracted from the *Infrared Space Observatory* (*ISO*) and *Spitzer* archives.

Three objects (IC 418, HR 4049, and NGC 7023) in our sample were observed between 1996 June and 1998 February using the *ISO Short-Wavelength Spectrometer* (SWS). The observations were performed using the Astronomical Observation Template (AOT) 01 mode at various speeds with spectral resolving power ($\lambda/\Delta\lambda$) ranging from 500 to 1600, covering a wavelength range of 2.4–45.2 μm . The aperture sizes are 14'' \times 20'' for the 2.4–12 μm region and 14'' \times 27'' for the 11–28 μm band in the SWS module, respectively, and the exposures on sources of the measurements varied between 1834s and 6538s,

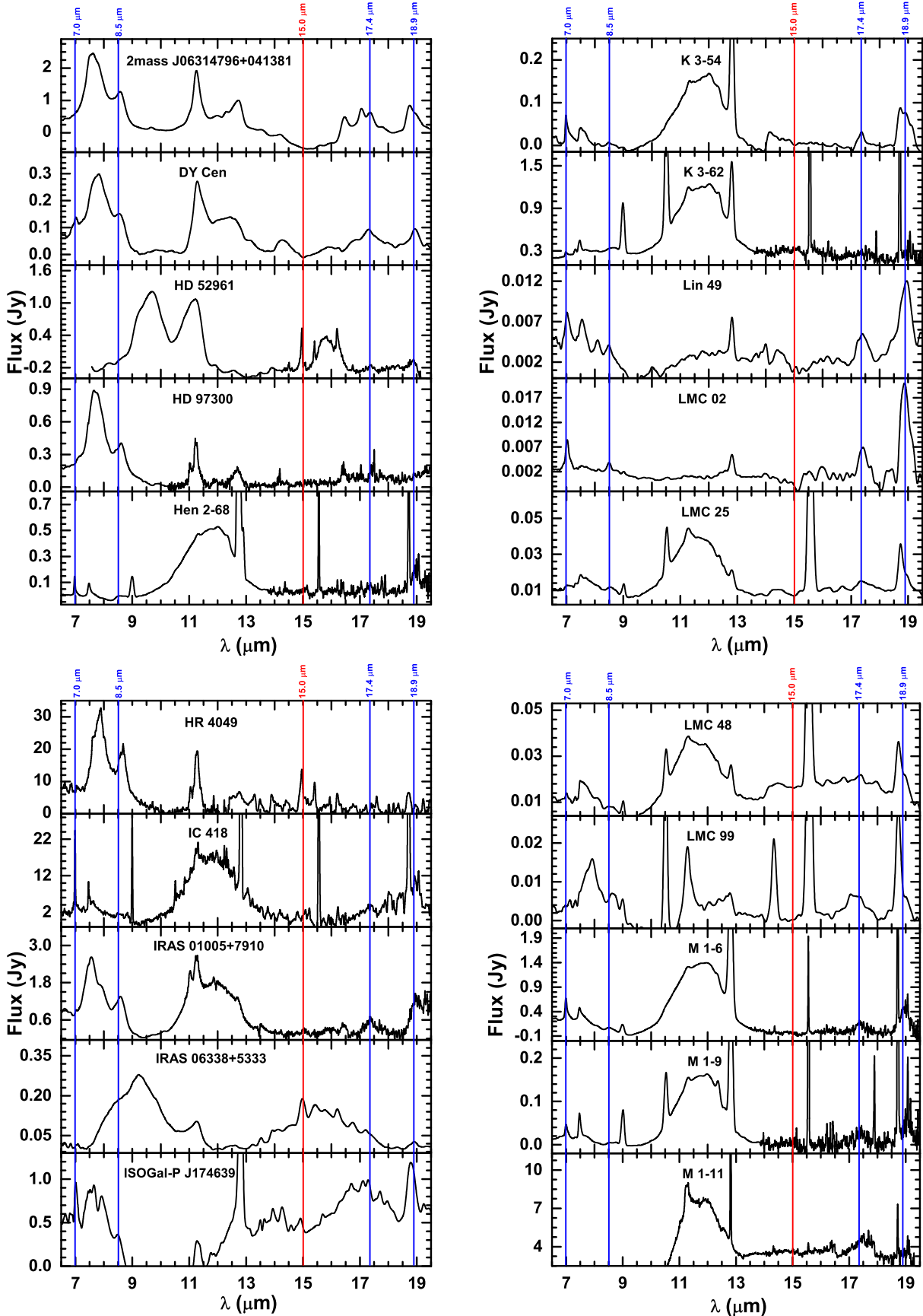


Figure 17. Continuum-subtracted mid-infrared spectra of known C_{60} sources in the wavelength range of $6.5\text{--}19.5\ \mu\text{m}$. The blue and red lines indicate the positions of the C_{60} bands and the $15\ \mu\text{m}$ feature, respectively.

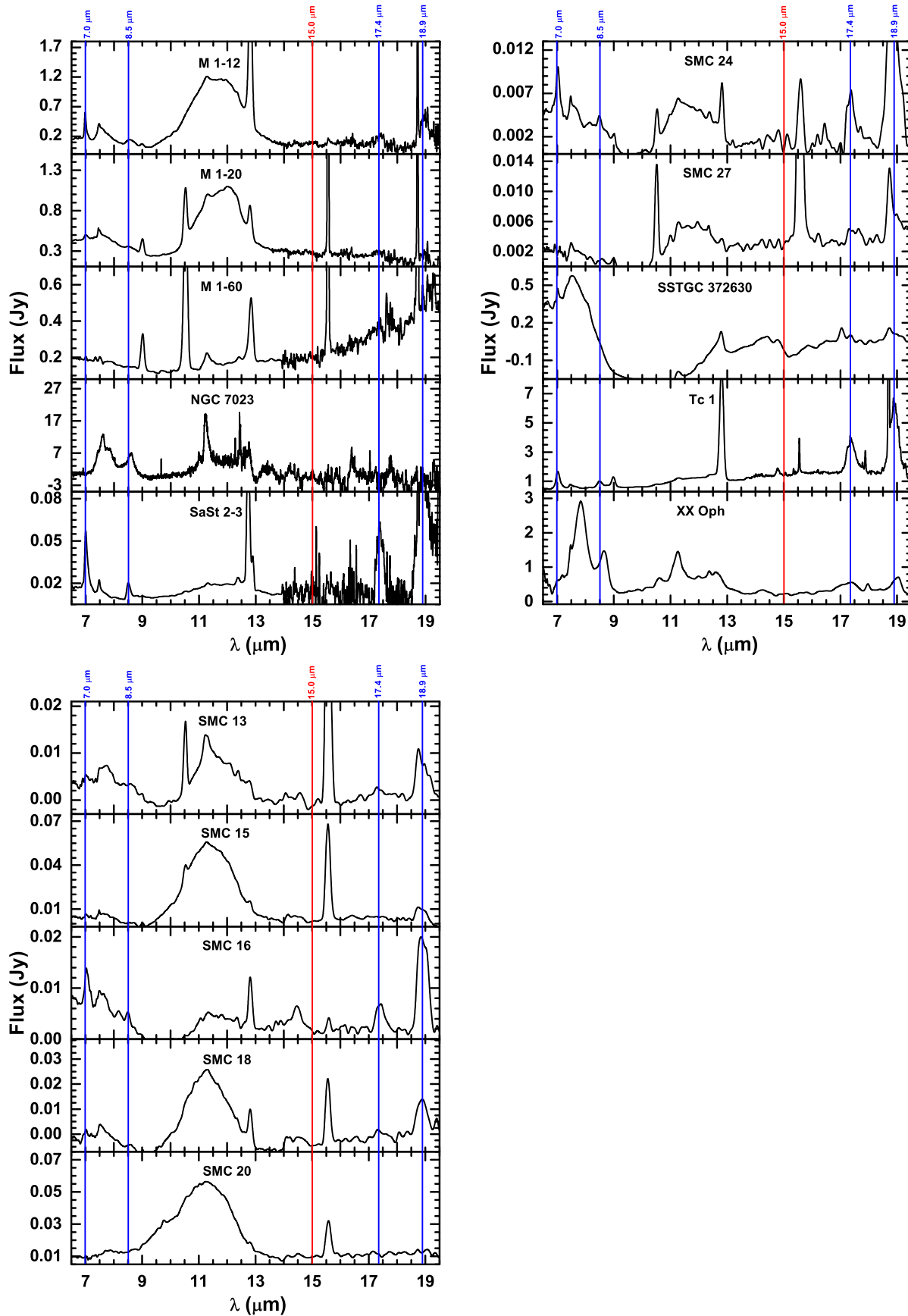


Figure 17. (Continued.)

depending on the source brightnesses. The observations for all objects are centered on the core positions. The data reduction and calibration were performed through the standard procedure.

The mid-infrared spectra of the other 32 objects in Table 1 are obtained with the *Infrared Spectrograph* (IRS) on board the *Spitzer Space Telescope*. All of these objects were observed using the Short-Low (SL) and Short-High (SH) modules, covering the wavelength coverage of 5.2–19.6 μm with spectral dispersion of $R \sim 64$ –600. The aperture sizes are $3''\!6 \times 57''$ and $4''\!7 \times 11''\!3$ in SL and SH modules, respectively, and the total integration times of IRS observations range from 39 s to 2462 s, depending on the sources' expected mid-infrared fluxes. Data were reduced starting with basic calibrated data from the Spitzer Science Center's pipeline version s18.7 and were run through the IRS-CLEAN program to remove rogue pixels. Then we employed point-source spectral extractions to extract spectra using the Spectral Modeling, Analysis and Reduction Tool. A final spectrum was produced using the combined IRS observations to improve the S/N.

Figure 17 shows the spectra of the 35 objects. The continua were fitted with a third-order polynomial and subtracted from the spectra. The positions of the four C₆₀ bands and the 15 μm feature are marked with vertical lines. The search results are given in column 3 of Table 1, where ticks indicate tentative detections and colons indicate marginal or uncertain detections.

Appendix B The Spatially Resolved Spectra of NGC 7023

Infrared spectroscopic observations of NGC 7023 were carried out by the IRS on board the *Spitzer Space Telescope* in the spectral mapping mode on 2004 August (AOR 3871232). We extracted five high-resolution spectra at different positions, which were taken with the SH module covering the wavelength range of 9.9–19.6 μm . The slit sizes are $4''\!7 \times 11''\!3$ and the exposure time of each spectrum is 20 s. Data were reduced using basic calibrated data from the Spitzer Science Center's pipeline version s18.8 and the IRS-CLEAN program for removing rogue pixels was performed. A low-order polynomial fit was applied to subtract the continuum. These spatially resolved spectra are shown in Figure 15.

We note that the 15 μm feature is detected in both the *ISO* (Figure 17) and *Spitzer* (Figure 15) spectra of NGC 7023.

References

- Bernard-Salas, J., Cami, J., Peeters, E., et al. 2012, *ApJ*, **757**, 41
 Berné, O., Mulas, G., & Joblin, C. 2013, *A&A*, **550**, L4
 Berné, O., & Tielens, A. G. G. M. 2012, *PNAS*, **109**, 401
 Bonchev, D., & Rouvray, D. H. 1995, Chemical Group Theory: Techniques and Applications (London: Gordon and Breach)
 Brieva, A. C., Gredel, R., Jäger, C., Huisken, F., & Henning, T. 2016, *ApJ*, **826**, 122
 Cami, J., Bernard-Salas, J., Peeters, E., & Malek, S. E. 2010, *Sci*, **329**, 1180
 Campbell, E. K., Holz, M., Gerlich, D., & Maier, J. P. 2015, *Natur*, **523**, 322
 Campbell, E. K., Holz, M., & Maier, J. P. 2016a, *ApJL*, **826**, L4
 Campbell, E. K., Holz, M., Maier, J. P., et al. 2016b, *ApJ*, **822**, 17
 Cataldo, F., & Iglesias-Groth, S. 2009, *MNRAS*, **400**, 291
 Cataldo, F., & Iglesias-Groth, S. 2010, Fullerenes: The Hydrogenated Fullerenes (Berlin: Springer)
 Cataldo, F., Strazzulla, G., & Iglesias-Groth, S. 2009, *MNRAS*, **394**, 615
 Díaz-Luis, J. J., García-Hernández, D. A., Kameswara Rao, N., Manchado, A., & Cataldo, F. 2015, *A&A*, **573**, A97
 Díaz-Luis, J. J., García-Hernández, D. A., Manchado, A., & Cataldo, F. 2016, *A&A*, **589**, A5
 Evans, A., van Loon, J. T., Woodward, C. E., et al. 2012, *MNRAS*, **421**, L92
 Foing, B. H., & Ehrenfreund, P. 1994, *Natur*, **369**, 296
 Frisch, M. J., Trucks, G. W., Schlegel, J. B., et al. 2009, Gaussian 09, Revision C.01 (Wallingford, CT: Gaussian, Inc.)
 Fulara, J., Jakobi, M., & Maier, J. P. 1993, *CPL*, **211**, 227
 García-Hernández, D. A., Iglesias-Groth, S., Acosta-Pulido, J. A., et al. 2011a, *ApJL*, **737**, L30
 García-Hernández, D. A., Kameswara Rao, N., & Lambert, D. L. 2011b, *ApJ*, **729**, 126
 García-Hernández, D. A., Manchado, A., García-Lario, P., et al. 2010, *ApJL*, **724**, L39
 García-Hernández, D. A., Villaver, E., García-Lario, P., et al. 2012, *ApJ*, **760**, 107
 Gielen, C., Cami, J., Bouwman, J., Peeters, E., & Min, M. 2011, *A&A*, **536**, A54
 Goldshleger, N. F., & Moravsky, A. P. 1997, *RuCRv*, **66**, 323
 Herbig, G. H. 2000, *ApJ*, **542**, 334
 Iglesias-Groth, S., & Esposito, M. 2013, *ApJL*, **776**, L2
 Iglesias-Groth, S., García-Hernández, D. A., Cataldo, F., & Manchado, A. 2012, *MNRAS*, **423**, 2868
 Jensen, F. 2001, *JChPh*, **115**, 9113
 Jensen, F. 2002, *JChPh*, **116**, 7372
 Kroto, H. W., Heath, J. R., Obrien, S. C., Curl, R. F., & Smalley, R. E. 1985, *Natur*, **318**, 162
 Kwok, S. 2004, *Natur*, **430**, 985
 Kwok, S., Volk, K., & Bernath, P. 2001, *ApJL*, **554**, L87
 Kwok, S., Volk, K., & Hrivnak, B. J. 1989, *ApJL*, **345**, L51
 Laury, M. L., Carlson, M. J., & Wilson, A. K. 2012, *JCoCh*, **33**, 2380
 Maltseva, E., Petrignani, A., Candian, A., et al. 2015, *ApJ*, **814**, 23
 Micelotta, E. R., Jones, A. P., Cami, J., et al. 2012, *ApJ*, **761**, 35
 Omont, A. 2016, *A&A*, **590**, A52
 Otsuka, M., Kemper, F., Cami, J., Peeters, E., & Bernard-Salas, J. 2014, *MNRAS*, **437**, 2577
 Otsuka, M., Kemper, F., Hyung, S., et al. 2013, *ApJ*, **764**, 77
 Otsuka, M., Kemper, F., Leal-Ferreira, M. L., et al. 2016, *MNRAS*, **462**, 12
 Pauzat, F. 2011, in EAS Publications Ser. 46, PAHs and the Universe: A Symposium to Celebrate the 25th Anniversary of the PAH Hypothesis, ed. C. Joblin & A. G. G. M. Tielens (Les Ulis: EDP Sciences), **75**
 Pauzat, F., Pilmé, J., Toulouse, J., & Ellinger, Y. 2010, *JChPh*, **133**, 054301
 Pauzat, F., Talbi, D., & Ellinger, Y. 1995, *A&A*, **293**, 263
 Pogulay, A. V., Abzalimov, R. R., Nasibullaev, S. K., et al. 2004, *IJMSP*, **233**, 165
 Roberts, K. R. G., Smith, K. T., & Sarre, P. J. 2012, *MNRAS*, **421**, 3277
 Rüchardt, C., Gerst, M., Ebenhoch, J., et al. 1993, *Agnew. Chem. Int. ed. Engl.*, **32**, 584
 Sadjadi, S., Zhang, Y., & Kwok, S. 2015, *ApJ*, **801**, 34
 Sellgren, K., Werner, M. W., Ingalls, J. G., et al. 2010, *ApJL*, **722**, L54
 Snow, T. P., & Seab, C. G. 1989, *A&A*, **213**, 291
 Strelnikov, D., Kern, B., & Kappes, M. M. 2015, *A&A*, **584**, A55
 Volk, K., Kwok, S., & Hrivnak, B. J. 1999, *ApJL*, **516**, L99
 Walker, G. A. H., Bohlender, D. A., Maier, J. P., & Campbell, E. K. 2015, *ApJL*, **812**, L8
 Webster, A. 1992, *MNRAS*, **257**, 463
 Webster, A. 1995, *MNRAS*, **277**, 1555
 Werner, M. W., Uchida, K. I., Sellgren, K., et al. 2004, *ApJS*, **154**, 309
 Zerenturk, A., & Berber, S. 2012, *SSCom*, **152**, 1522
 Zhang, Y., & Kwok, S. 2011, *ApJ*, **730**, 126
 Zhang, Y., & Kwok, S. 2013, *EP&S*, **65**, 1069
 Zhang, Y., Kwok, S., & Hrivnak, B. J. 2010, *ApJ*, **725**, 990
 Zinner, E. 1998, *AREPS*, **26**, 147
 Zvereva, E. E., Shagidullin, A. R., & Katsyuba, S. A. 2011, *JPCA*, **115**, 63